Research Square

Preprints are preliminary reports that have not undergone peer review.
They should not be considered conclusive, used to inform clinical practice,
or referenced by the media as validated information.

Climate-Based Zoning Reveals Regional Differences in Potential Evapotranspiration Dynamics and Climatic Controls in Northeast China

Mingqian Li
Institute of Disaster Prevention
Runqing Yan
Institute of Disaster Prevention
He Wang
whnuo2009@163.com
Institute of Disaster Prevention

Research Article

Keywords: Potential evapotranspiration, K-means clustering analysis, Sensitivity analysis, Contribution rate, Northeast China

Posted Date: November 16th, 2026

DOI: https://doi.org/10.21203/rs.3.rs-10993863/v1

License: This work is licensed under a Creative Commons Attribution 4.0 International License.
Read Full License

Climate-Based Zoning Reveals Regional Differences in Potential Evapotranspiration Dynamics and Climatic Controls in Northeast China

Mingqian Li[a,b], Runqing Yan[a,b], He Wang[a,b]*

[a] School of Environmental and Disaster Management, Institute of Disaster Prevention, Langfang 065201, China

[b] Hebei Key Laboratory of Resource and Environmental Disaster Mechanism and Risk Monitoring, Sanhe 065201, China;

*Corresponding author. E-mail: whnuo2009@163.com

ABSTRACT

Reference evapotranspiration (ET_0) is an essential indicator of atmospheric evaporative demand and plays an important role in understanding regional water-energy interactions under climate change. However, the spatial heterogeneity of ET_0 responses and the dominant climatic controls in regions with complex topography remain insufficiently understood. This study developed an integrated framework combining climate-based K-means clustering, trend analysis, sensitivity assessment, and contribution analysis to investigate ET_0 variations in Northeast China. Daily meteorological observations from 106 stations during 1960–2020 were used to estimate ET_0 using the FAO-56 Penman–Monteith equation. The study area was objectively divided into four homogeneous subregions based on geographic and climatic characteristics. Results showed that air temperature increased significantly across all subregions, whereas wind speed, relative humidity, and sunshine duration generally decreased. Despite regional warming, ET_0 exhibited contrasting responses, with decreasing trends in Zones I and II, a weak increasing trend in Zone III, and a significant increase in Zone IV. Sensitivity analysis revealed that relative humidity exerted the strongest influence on ET_0, followed by wind speed and sunshine duration, while temperature showed the weakest sensitivity. The sign and magnitude of temperature sensitivity varied among subregions, and the negative coefficient in the high-latitude zone may partly reflect the normalization effect under cold climatic conditions rather than a direct physical suppression of ET_0 by warming. Contribution analysis further demonstrated that long-term ET_0 changes resulted from the combined effects of multiple climatic factors rather than temperature change alone. In particular, declining wind speed and reduced sunshine duration offset warming-related increases in evaporative demand in Zones I and II, leading to an evaporation paradox-like phenomenon. These findings highlight the importance of climate-based regionalization and integrated attribution approaches for understanding heterogeneous ET_0 responses under climate change.

Keywords: Potential evapotranspiration, K-means clustering analysis, Sensitivity analysis, Contribution rate, Northeast China,

HIGHLIGHTS

- Climate-based K-means clustering identified four homogeneous subregions with distinct hydrothermal characteristics in Northeast China.
- ET_0 responses to climate change showed strong regional heterogeneity despite widespread warming.
- Contribution analysis separated climatic sensitivity from actual driving effects on long-term ET_0 changes.
- An evaporation paradox-like phenomenon was mainly associated with reduced aerodynamic and radiation forcing under warming conditions.

1 Introduction

Climate change, characterized by persistent global warming and alterations in atmospheric circulation, has profoundly affected terrestrial ecosystems, agricultural production, and regional hydrological processes worldwide. In China, climate change has substantially modified hydrothermal conditions, thereby influencing water availability, ecological sustainability, and agricultural management (Zeng et al., 2021). As a key component of the terrestrial water cycle, evapotranspiration (ET) regulates the exchange of water and energy between the land surface and atmosphere. Reference evapotranspiration (ET_0), representing the atmospheric evaporative demand under standardized surface conditions, provides an essential indicator for evaluating regional water balance, irrigation requirements, and hydrological responses to climate variability. Therefore, understanding the spatiotemporal variations and climatic controls of ET_0 is fundamental for assessing the impacts of climate change on water resources.

The Penman–Monteith equation recommended by the Food and Agriculture Organization (FAO-56) is currently the most widely applied approach for estimating ET_0 because it integrates the effects of multiple meteorological variables, including temperature, humidity, radiation, and wind speed (Allen et al., 1998). Based on this framework, numerous studies have investigated long-term ET_0 variations across different climatic regions. Increasing ET_0 trends have been reported in many regions, such as the Nile River Basin, where annual and seasonal ET_0 increased during recent decades (Onyutha, 2016), and the Malaysian Peninsula, where increasing minimum temperature was identified as an important contributor to enhanced evaporative demand (Pour et al., 2020). Similar increasing trends have also been observed in Spain and several regions of China (Vicente-Serrano et al., 2014; Liu et al., 2010; Li et al., 2017). However, ET_0 does not always increase under global warming conditions. Declining ET_0 trends have been observed in regions such as central Iran, India, and eastern China, mainly associated with reductions in wind speed and increases in relative humidity (Dinpashoh et al., 2011; Chattopadhyay and Hulme, 1997; Qin et al., 2021). This phenomenon, commonly referred to as the "evaporation paradox", highlights the complexity of ET_0 responses and indicates that warming alone cannot fully explain changes in atmospheric evaporative demand.

To better understand the mechanisms controlling ET_0 variations, previous studies have examined the sensitivity and contribution of individual meteorological factors. These investigations have demonstrated that the dominant controlling factors vary considerably among seasons and

climate regimes. For example, minimum temperature was identified as the major factor affecting summer ET_0 on the Korean Peninsula, whereas relative humidity played a stronger role during other seasons (Ghafouri-Azar and Lee, 2023). Similarly, maximum temperature dominated ET_0 variations during warm seasons in Japan, while humidity became more influential in winter (Ghiami-Shomami et al., 2019). Studies conducted across Australia further revealed that ET_0 sensitivity patterns differed substantially between cold, humid, and arid regions, with temperature, wind speed, solar radiation, and humidity exhibiting contrasting influences depending on climatic conditions (Guo et al., 2017). These findings demonstrate that ET_0 responses are highly spatially heterogeneous and cannot be adequately characterized by a single dominant climatic factor.

Despite substantial progress, several limitations remain in current ET_0 sensitivity studies. First, many previous investigations have relied on individual analytical approaches, such as sensitivity analysis or correlation-based methods, without integrating sensitivity with contribution assessment. Consequently, the relative importance of meteorological factors in explaining actual ET_0 changes remains uncertain. Second, spatial heterogeneity has often been evaluated according to administrative boundaries or predefined geographical units, which may not adequately represent regional differences in climate and environmental conditions. For large regions with strong climatic gradients, objective climate-based zoning approaches are required to identify homogeneous regions and reveal distinct ET_0 response mechanisms. Third, although considerable attention has been given to basin-scale or local-scale studies, comprehensive analyses that integrate spatial clustering, trend detection, sensitivity evaluation, and contribution quantification remain limited, particularly in regions characterized by strong climatic transitions.

Northeast China provides an ideal region for investigating these issues. As one of the world's major black soil regions and an important agricultural production base, this area plays a crucial role in national food security. Meanwhile, Northeast China is characterized by pronounced climatic gradients, diverse topography, and substantial seasonal variability, which may result in different ET_0 responses among subregions. Previous studies have improved understanding of evapotranspiration variations in individual river basins or local areas within Northeast China (Liang et al., 2008; Shi et al., 2022). However, a comprehensive assessment of ET_0 variations across the entire Northeast region remains insufficient. In particular, the spatial differentiation of dominant climatic controls and the mechanisms underlying anomalous ET_0 responses, such as decreasing ET_0

under warming conditions, require further investigation.

To address these knowledge gaps, this study develops an integrated framework combining climate-based spatial zoning, trend analysis, sensitivity evaluation, and contribution assessment to investigate ET_0 variations in Northeast China. Unlike previous studies based primarily on administrative divisions or individual climatic variables, this study applies the K-means clustering method to objectively identify subregions with similar climatic and environmental characteristics, thereby improving the representation of spatial heterogeneity in ET_0 responses. Furthermore, sensitivity analysis is combined with contribution rate assessment to distinguish between climatic factors that are highly sensitive and those that exert dominant practical influences on ET_0 changes. This approach provides new insights into regional differences in ET_0 dynamics and improves understanding of the mechanisms driving evaporation paradox phenomena.

Using daily meteorological observations (temperature, relative humidity, sunshine duration, and wind speed) from 106 meteorological stations in Northeast China during 1960–2020, this study aims to: (1) identify climate-homogeneous subregions using the K-means clustering approach; (2) characterize spatial and temporal trends of ET_0 and associated meteorological variables using the Mann–Kendall test and Sen's slope estimator; and (3) quantify the sensitivity and contribution of meteorological factors to ET_0 variations across different subregions.

2 Data and methods

2.1 Study area

Northeast China is located in the northeastern part of China and represents a transition zone characterized by complex topography and pronounced climatic gradients. The region is dominated by a combination of plains, hills, and mountains. The Changbai Mountains are distributed in the east, the Lesser Khingan Range extends across the north, and the Greater Khingan Range forms the western boundary. These mountain systems surround the extensive Northeast Plain, creating a distinctive three-zone geomorphological pattern (Figure 1). The outer zone mainly consists of low-elevation areas along the Heilongjiang, Ussuri, Tumen, and Yalu River basins; the middle zone is characterized by mountains and hills; and the inner zone corresponds to the broad Northeast Plain. This complex topographic configuration contributes to substantial spatial differences in regional climate conditions and hydrothermal processes.

The climate of Northeast China spans cold temperate, mid-temperate,

and warm temperate zones from north to south. Influenced by the East Asian monsoon and the gradual weakening of maritime influence from east to west, the region exhibits clear gradients in temperature and moisture conditions. The eastern and southeastern areas are relatively humid due to stronger oceanic influence, whereas the western areas are generally drier. Summers are warm and humid with concentrated precipitation, while winters are long, cold, and dry, resulting in strong seasonal variations in radiation, temperature, humidity, and wind conditions. These pronounced climatic gradients provide diverse environmental conditions for investigating the spatial variability of reference evapotranspiration (ET_0) and its climatic controls.

The region contains an extensive river network, with major rivers including the Heilongjiang, Songhua, and Liao rivers. Precipitation is highly seasonal, with approximately 60–70% of annual rainfall occurring during July and August, corresponding to the main agricultural growing season. Meanwhile, prolonged low temperatures in winter lead to frozen soil and river ice conditions, substantially limiting evapotranspiration during the cold season. The combined effects of topographic complexity, seasonal climate variation, and uneven hydrothermal conditions result in considerable spatial heterogeneity in ET_0 across Northeast China, making it an appropriate region for examining climate-driven variations and regional differences in evapotranspiration responses.

2.2 Data sources

Daily meteorological observations from 106 stations in Northeast China during 1960–2020 were obtained from the China Meteorological Data Service Center (https://data.cma.cn/). The dataset includes maximum and minimum air temperatures, which were used to calculate mean temperature (TEM), wind speed (WIND) measured at 10 m height, relative humidity (RH), precipitation (PRE), and sunshine duration (SSD), which was used as a proxy for solar radiation. Following the wind profile adjustment procedure recommended in FAO Paper No. 56, 10-m wind speed observations were converted to wind speed at 2 m height for reference evapotranspiration (ET_0) estimation. The spatial distribution of the selected meteorological stations is presented in Figure 1.



Fig.1 Location of the study area, distribution of weather stations, and climatic subregions in Northeast China.

2.3 K-means Clustering Analysis

The K-means clustering algorithm, originally proposed by MacQueen (1967), is an unsupervised classification method that partitions datasets into groups based on similarities among samples. It has been widely applied in environmental and hydroclimatic studies for identifying homogeneous regions with similar physical characteristics (Dikbas et al., 2013; Ikotun et al., 2023). Unlike predefined administrative or geographical divisions, clustering-based regionalization can objectively identify spatial units with comparable climatic conditions, which is particularly suitable for regions characterized by strong environmental gradients (Hu et al., 2023).

The basic principle of K-means clustering is to minimize the within-cluster sum of squared errors by assigning samples to the nearest cluster centroid. Given a dataset containing n samples (x_1, x_2, ..., x_n), k initial centroids (μ_1, μ_2, ..., μ_k) are randomly selected. The objective function is defined as:

$$J(c,\mu) = \min \sum_{i=1}^{M} \left\| x_i - \mu_{c_i} \right\|^2 \quad (1)$$

where J represents the total within-cluster variance, and $||x_i-\mu_j||$

represents the Euclidean distance between sample x_i and centroid μ_j. During each iteration, samples are assigned to the cluster with the minimum distance from the corresponding centroid:

$$c_i^t <- \arg\min_k \left\| x_i - \mu_k^t \right\|^2 \quad (2)$$

After sample assignment, the centroid of each cluster is recalculated as the mean value of all samples belonging to that cluster:

$$\mu_k^{(t+1)} <- \arg\min_u \sum_{i:c_i^t=k}^{b} \left\| x_i - \mu \right\|^2 \quad (3)$$

The iterative procedure continues until the objective function converges and no further changes occur in cluster membership.

Northeast China exhibits substantial spatial heterogeneity due to its complex topography, distinct latitudinal climate gradients, and varying hydrothermal conditions. Therefore, traditional regional divisions based on administrative boundaries may not fully represent differences in climatic controls on reference evapotranspiration (ET_0). In this study, K-means clustering was applied to objectively classify meteorological stations into homogeneous subregions. The clustering variables included geographic characteristics (latitude, longitude, and elevation) and key meteorological factors affecting ET_0, including TEM, RH, SSD, and WIND. Before clustering, all variables were standardized using z-score normalization to eliminate the influence of different units and magnitudes among variables. Considering both clustering performance and the physical interpretability of regional climate patterns, four clusters were selected as the optimal classification.

2.4 Calculation of ET_0 Using the Penman-Monteith Equation

The FAO-56 Penman–Monteith equation was used to estimate ET_0. The method integrates net radiation, air temperature, atmospheric humidity, and wind speed under standardized reference-surface conditions (Allen *et al.* 1998; Liu *et al.* 2010; Sun *et al.* 2020). The calculation formula is expressed as:

$$ET_0 = \frac{0.408\Delta(R_n - G) + \gamma \frac{900}{T+273} u_2 (e_s - e_a)}{\Delta + \gamma(1 + 0.34u_2)} \quad (4)$$

where: T represents the daily mean air temperature at 2 m height above ground (℃); R_n denotes the net radiation at the crop surface (MJ m^{-2} day^{-1}); G refers to the soil heat flux density (MJ m^{-2} day^{-1}); γ is the psychrometric constant (kPa $℃^{-1}$); u_2 indicates the WIND at 2 m height (m s^{-1}); e_s signifies

the mean saturation vapor pressure (kPa); e_a represents the actual vapor pressure (kPa) and e_s-e_a is the saturation vapor pressure deficit (kPa); Δ stands for the slope of the saturation vapor pressure-temperature curve (kPa $^{\circ}C^{-1}$).

2.5 Mann-Kendall Trend Test

The Mann–Kendall (MK) test is a widely used non-parametric method for detecting monotonic trends in hydroclimatic time series (Fang et al., 2019). Compared with parametric approaches, the MK test does not require assumptions regarding data normality or linearity, making it suitable for analyzing long-term variations in meteorological variables (Zhao et al., 2020).

For a given time series $X = \{x_1, x_2, x_3, ..., x_n\}$ with length n, the MK test statistic S can be expressed as (Fang *et al.* 2019):

$$S = \sum_{i=1}^{n-1} \sum_{j=i+1}^{n} \operatorname{sgn}(x_i - x_j), \quad \operatorname{sgn}(x_i - x_j) = \begin{cases} 1, & x_j > x_i \\ 0, & x_j = x_i \\ -1, & x_j < x_i \end{cases} \tag{5}$$

where: n represents the number of observations; x_i and x_j denote the i-th and j-th ($j>i$) observations in the time series, respectively.

For a dataset where all values are distinct, the variance is given by:

$$\operatorname{Var}(S) = \frac{n(n-1)(2n+5)}{18} \tag{6}$$

The standardized test statistic Z is calculated as:

$$Z = \begin{cases} \dfrac{S-1}{\sqrt{\operatorname{var}(S)}}, & S > 0 \\ 0, & S = 0 \\ \dfrac{S+1}{\sqrt{\operatorname{var}(S)}}, & S < 0 \end{cases} \tag{7}$$

The results demonstrate statistical significance at the 1%, 5%, and 10% levels when $|Z| > 2.576$, $|Z| > 1.96$, and $|Z| > 1.645$, respectively. A positive Z value indicates an upward trend, while a negative Z value represents a downward trend (Ozocak *et al.* 2024).

2.6 Sen's Slope Estimator

The Sen's slope estimation method (Sen, 1968) was employed to analyze monotonic trends by calculating the slope β of the trend line in the time series. For a given time series $X = (x_1, x_2, ..., x_n)$, the slope β is computed as follows (Aschale *et al.* 2023; Wang *et al.* 2019):

$$\beta = \text{Median}(\frac{x_j - x_i}{j - i}), \forall j > i \quad (8)$$

where: *Median* represents the median function.

A positive β indicates an increasing tendency, whereas a negative β indicates a decreasing tendency. The statistical significance of the trend was assessed using the Mann–Kendall test.

2.7 Sensitivity Analysis

The sensitivity coefficient method, introduced by McCuen in 1974 as an approach for sensitivity and error analysis (McCuen, 1974), provides a quantitative means to assess the relative influence of variations in meteorological factors on evapotranspiration rate calculations (Rim, 2004). The sensitivity coefficient is defined as(Ghafouri-Azar & Lee, 2023; Zhao *et al.* 2020):

$$s_{vi} = \lim_{\Delta vi \to 0} \frac{\Delta ET_0 / ET_0}{\Delta v_i / v_i} = \frac{\partial ET_0}{\partial v_i} \times \frac{v_i}{ET_0} \quad (9)$$

where: s_{vi} represents the sensitivity coefficient of the *i*-th meteorological factor and v_i denotes the *i*-th meteorological factor.

The absolute value of s_{vi} was used to evaluate the magnitude of ET_0 sensitivity to each meteorological factor. A larger $|s_{vi}|$ indicates that ET_0 exhibits a stronger response to changes in the corresponding climatic factor, whereas a smaller $|s_{vi}|$ indicates a weaker response.

2.8 Contribution Rate Method

The contribution rate method combines the sensitivity coefficient and the long-term relative change rate of individual meteorological factors to quantify their relative contributions to ET_0 variation (Yin et al., 2010). Specifically, the product of the sensitivity coefficient and the relative change rate represents the contribution of each meteorological factor to long-term ET_0 changes. This relationship can be expressed as follows (Aschale et al., 2023; Li et al., 2017):

$$C_{vi} = s_{vi} \cdot RC_{vi}, \quad RC_{vi} = \frac{n \times \text{Trend}_{v_i}}{|av_i|} \times 100\% \quad (10)$$

where C_{vi} represents the contribution rate of meteorological factor vi to ET_0 variation, s_{vi} denotes the sensitivity coefficient of vi, and RC_{vi} represents the relative change rate of vi; n represents the length of the study period (years), a_{vi} represents the multi-year mean value of vi, and

$Trend_{vi}$ represents the long-term tendency rate of vi.

3. Results and Analysis

3.1 Subregion Division of Northeast China

The K-means clustering algorithm classified Northeast China into four homogeneous subregions based on geographic characteristics and key climatic variables (Figure 1). Zone Ⅰ is mainly distributed across the central-southern Songliao Plain, representing the low-elevation plain area. Zone Ⅱ is located primarily within the Greater Khingan Mountains, characterized by relatively high elevation and continental climatic conditions. Zone Ⅲ is concentrated in the Changbai Mountains and adjacent eastern mountainous areas, whereas Zone Ⅳ occupies the northern high-latitude region extending along the junction between the Lesser Khingan and Changbai Mountains. The spatial patterns of these four clusters correspond well with the major geomorphological and climatic gradients of Northeast China.

The multi-year mean characteristics of each subregion are summarized in Table 1. The elevation gradient follows the order of Zone Ⅳ > Zone Ⅱ > Zone Ⅲ > Zone Ⅰ, consistent with the regional topographic pattern of surrounding mountains and a central plain. The climatic differences among subregions reflect the combined effects of elevation, latitude, atmospheric circulation, and topographic barriers. Zone Ⅲ exhibits the highest precipitation and relative humidity due to the influence of the Changbai Mountains and enhanced moisture transport from the surrounding oceanic region. In contrast, Zone Ⅰ is located in the interior plain and experiences relatively limited moisture supply, resulting in higher temperature and wind speed but lower precipitation. Zone Ⅱ is strongly influenced by the Greater Khingan Mountains, with high sunshine duration and relatively low humidity, indicating a dry continental climate. Zone Ⅳ, located at the highest latitude, has the lowest temperature and relatively weak evaporative demand due to prolonged cold conditions.

According to Table 1, Zone Ⅰ has the highest TEM and WIND, which contributes to its relatively high ET_0. Zone Ⅱ exhibits the highest SSD and intermediate ET_0, indicating the important role of available energy and atmospheric demand in mountainous areas. Despite having the highest precipitation and humidity, Zone Ⅲ shows the lowest ET_0 among the relatively warm regions because lower temperature and reduced atmospheric drying capacity constrain evapotranspiration. Zone Ⅳ has the lowest ET_0 due to its high latitude, low temperature, and short growing season. These results demonstrate that the spatial distribution of ET_0 in Northeast China is jointly controlled by thermal conditions, atmospheric

moisture, energy availability, and topographic effects.

The clustering results indicate that climate-based regionalization can effectively capture the spatial heterogeneity of hydrothermal conditions in Northeast China. Compared with traditional administrative divisions, the K-means approach provides a more physically meaningful framework for identifying regions with similar climatic controls, which is essential for further analysis of ET_0 trends, sensitivity, and dominant climatic drivers.

Table 1. Annual mean values of parameters for each zone

Zone	ET_0/mm	WIND/ $m \cdot s^{-1}$	RH/%	TEM/℃	SSD / $h \cdot d^{-1}$	PRE/mm	Climatic characteristics
Ⅰ	965.42	3.32	62.87	6.87	7.35	442.42	Hot and dry
Ⅱ	1034.28	2.93	52.94	6.18	7.86	525.34	Hot and moist
Ⅲ	792.27	2.63	68.26	4.99	6.59	654.03	Warm and humid
Ⅳ	718.49	2.60	66.62	-0.64	7.18	530.43	Cold and dry

3.2 Temporal Variation Characteristics of ET_0 and Meteorological Factors

Based on the climate-based subregional classification obtained from the K-means clustering method, the temporal variations of ET_0 and related meteorological factors were analyzed using annual time series (Figure 2), trend statistics (Table 2), and spatial distributions of trends (Figure 3).

The temporal evolution of meteorological factors exhibited consistent patterns among the four subregions, although their magnitudes varied spatially. TEM showed a significant increasing trend in all subregions ($p < 0.01$), indicating a persistent warming tendency across Northeast China. In contrast, WIND, RH, and SSD generally exhibited decreasing trends, suggesting concurrent changes in atmospheric circulation, moisture conditions, and energy availability. Among these factors, WIND exhibited the most consistent long-term decline. Although WIND showed a short-term rebound in some subregions during approximately 2010–2020, the Sen's slope over the entire 1960–2020 period remained significantly negative in all four subregions (Table 2). This long-term decline may reduce aerodynamic evapotranspiration demand, whereas decreasing RH may enhance atmospheric drying capacity and partially offset the effects of reduced wind speed and radiation.

The trend analysis results (Table 2) further revealed distinct regional differences in ET_0 responses. ET_0 showed decreasing trends in Zones Ⅰ and Ⅱ, although these trends were not statistically significant. In contrast, Zones Ⅲ and Ⅳ exhibited increasing ET_0 trends, with a significant increase observed in Zone Ⅳ ($p < 0.01$). These contrasting patterns indicate that regional warming does not uniformly translate into increased

ET_0, and that the combined effects of multiple climatic factors determine ET_0 variability.

Spatial distributions of trends (Figure 3) further demonstrated the heterogeneity of ET_0 changes across Northeast China. Negative ET_0 trends were mainly concentrated in parts of the central plain region, while significant positive trends were observed in the northern high-latitude region. The increasing ET_0 in Zone Ⅳ may be associated with enhanced thermal conditions and reduced atmospheric humidity under climate warming. Meanwhile, the relatively weak or decreasing ET_0 trends in Zones Ⅰ and Ⅱ may result from the compensating effects among temperature increases, declining wind speed, reduced sunshine duration, and changes in atmospheric moisture conditions.

These regional differences provide a more detailed perspective than previous analyses conducted at the scale of Northeast China as a whole. Liu et al. (2022) reported a nonsignificant increasing trend in annual ET_0 during 1960–2017, together with pronounced spatial differences related to elevation. The present K-means-based regionalization further demonstrates that such an overall trend masks contrasting subregional responses, with weak decreases in Zones I and II but increasing ET_0 in Zones III and IV. Overall, the temporal variations of ET_0 and meteorological factors demonstrate that the response of atmospheric evaporative demand to climate change is spatially heterogeneous in Northeast China. Further sensitivity and contribution analyses are required to identify the dominant climatic factors controlling these regional differences (Zhao et al., 2016).

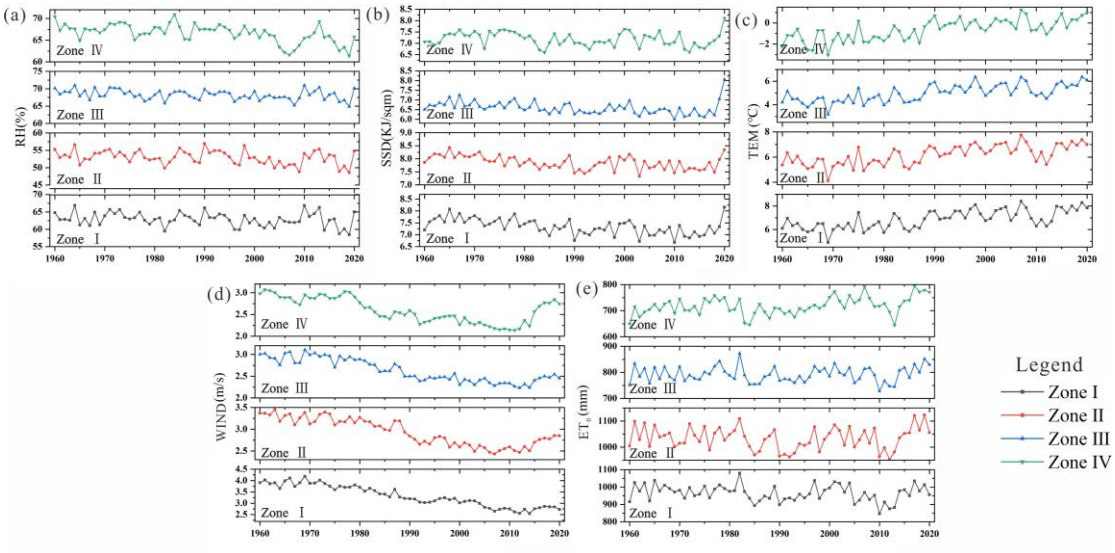


Fig.2 Interannual variations of meteorological factors across subregions (a. RH b. SSD c. TEM d. WIND e. ET_o)

Table 2. Sen's slope estimates and Mann–Kendall trend significance of ET_0

and meteorological factors across different subregions

Zone	WIND	RH	TEM	SSD	ET_0
I	-0.025***	-0.029*	0.030***	-0.010***	-0.537
II	-0.015***	-0.036**	0.029***	-0.007***	-0.063
III	-0.013***	-0.025***	0.028***	-0.006***	0.076
IV	-0.011***	-0.067***	0.039***	-0.003*	0.747***

Note: *, **, and *** indicate significant trends at the 90%, 95%, and 99% confidence levels based on the Mann–Kendall test, respectively.

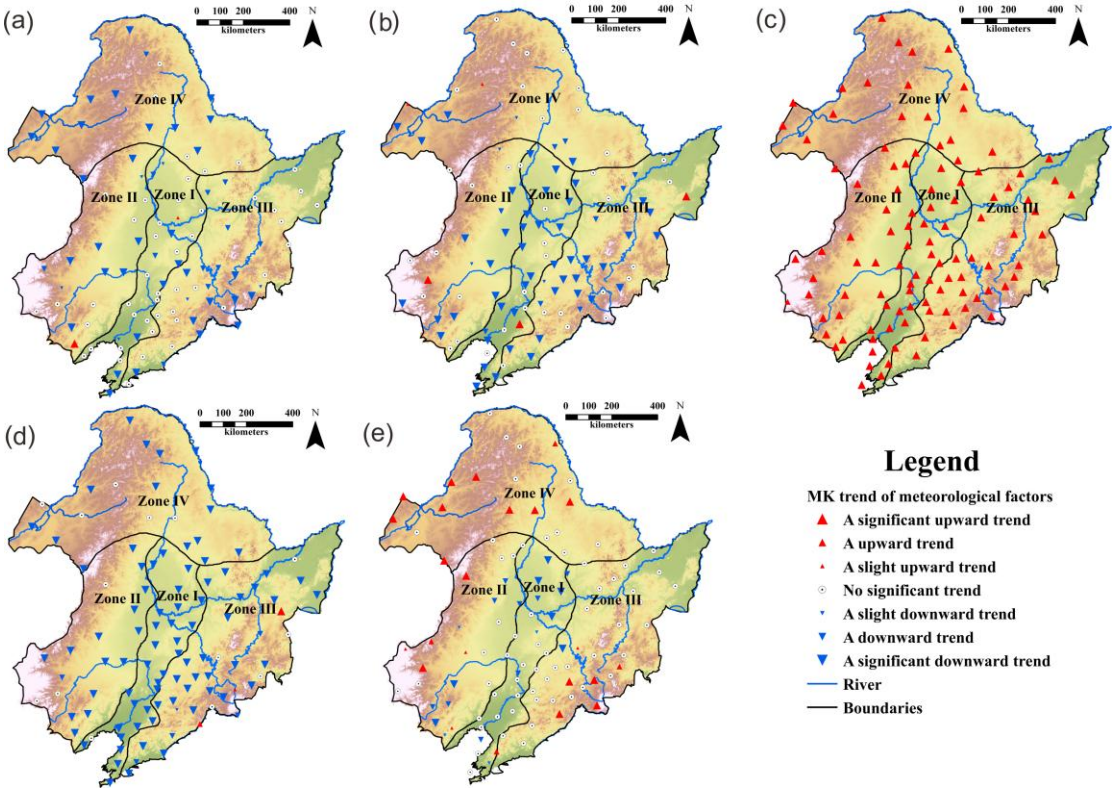


Fig.3 Spatial distribution of multi-year trends for meteorological factors across monitoring stations in Northeast China (a. RH. b. SSD. c. TEM. d. WIND. e. ET_0.)

3.3 Spatial Distribution Characteristics of ET_0 and Meteorological Factors

The spatial distributions of the multi-year mean ET_0 and associated meteorological factors across Northeast China are shown in Figure 4. Pronounced spatial heterogeneity was observed for ET_0, TEM, RH, SSD, and WIND, with their distribution patterns broadly corresponding to the climatic and topographic differences among the four subregions identified by K-means clustering.

ET_0 generally exhibited higher values in the southwestern and western parts of Northeast China and lower values toward the northern and northeastern areas. Among the four subregions, Zone II had the highest

multi-year mean ET_0 (1034.28 mm), followed by Zone Ⅰ (965.42 mm), Zone III (792.27 mm), and Zone Ⅳ (718.49 mm) (Table 1). The relatively high ET_0 in Zones Ⅰ and Ⅱ coincided spatially with relatively high TEM, SSD, and/or WIND and comparatively low RH, whereas the lower ET_0 in Zones III and IV was associated with cooler and more humid climatic conditions.

The individual meteorological factors also exhibited distinct spatial gradients. TEM showed a pronounced south-to-north decrease, with the highest mean value occurring in Zone I and the lowest in the high-latitude Zone Ⅳ. SSD was generally higher in the western part of the study area and decreased toward the east, with Zone Ⅱ exhibiting the highest regional mean. WIND was highest across the central plain, particularly in Zone Ⅰ, and was generally lower in the surrounding mountainous regions. In contrast, RH showed a less distinct directional gradient but was relatively high in the eastern mountainous and northern regions, with Zone Ⅲ exhibiting the highest regional mean RH.

Comparison with the regional topography (Figure 1) indicates that these spatial patterns are broadly consistent with the combined effects of latitude, elevation, and regional climatic conditions. Zone Ⅰ, dominated by low-elevation plains, was characterized by relatively high TEM and WIND. Zone Ⅱ, located mainly in the Greater Khingan Mountains, exhibited relatively high elevation, the highest SSD, and the lowest RH among the four subregions. Zone Ⅲ, covering the Changbai Mountains and adjacent eastern areas, was characterized by the highest RH and precipitation but relatively low SSD. Zone Ⅳ, located at higher latitudes and elevations, exhibited the lowest TEM and ET_0.

Overall, the spatial distribution of ET_0 did not correspond to any single meteorological factor but reflected the combined spatial variations in thermal conditions, atmospheric moisture, energy availability, and aerodynamic conditions. In particular, the contrasting climatic characteristics among the K-means-derived subregions provide a physical basis for examining regional differences in ET_0 sensitivity and the contributions of individual climatic factors in the subsequent analyses.

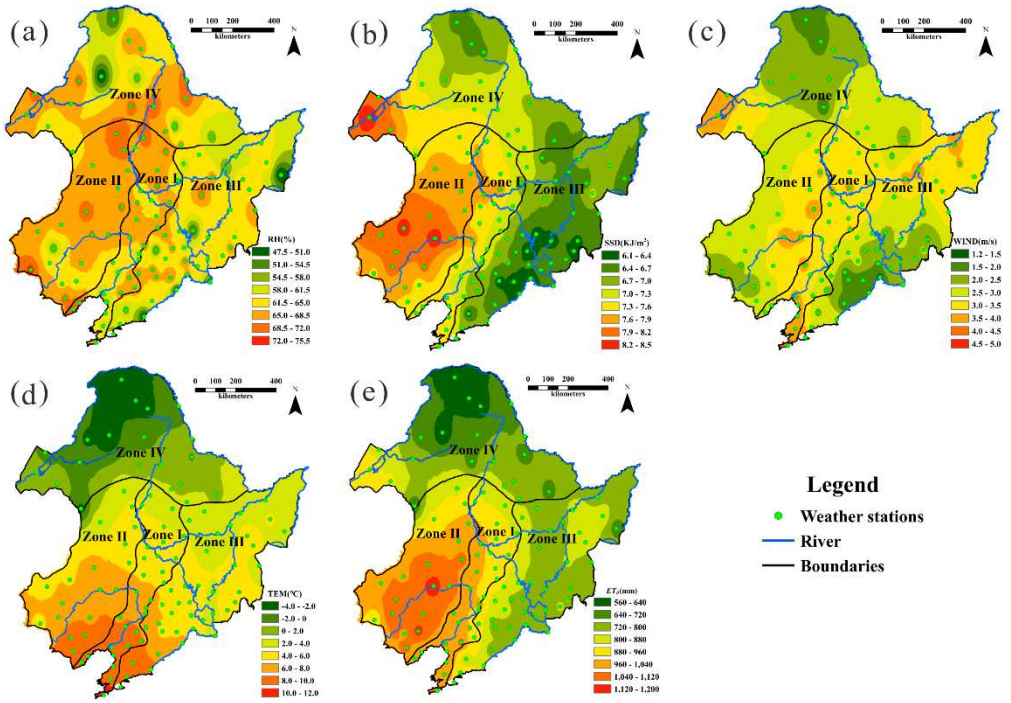


Fig.4 Spatial distribution map of multi-year mean value of meteorological factors and ET_0 in Northeast China

3.4 Sensitivity Analysis of Meteorological Factors

The temporal and spatial variations in the sensitivity coefficients of ET_0 to RH, SSD, TEM, and WIND are presented in Figures 5, Figures 6 and Table 3. The sensitivity coefficients varied both temporally and spatially, indicating that the response of ET_0 to individual meteorological factors was dependent on the prevailing climatic conditions rather than remaining constant throughout the study period. This temporal variability suggests that long-term climate change may alter not only the meteorological variables themselves but also the response of atmospheric evaporative demand to changes in these variables.

The RH sensitivity coefficients remained negative throughout the study period in all four subregions (Figure 5a), indicating that increasing RH tended to reduce ET_0. However, the coefficients generally shifted toward less negative values over time, particularly in Zones Ⅰ, Ⅲ, and Ⅳ. Because the RH sensitivity coefficients are negative, this upward trend corresponds to a decrease in their absolute magnitude, implying a gradual weakening of the relative sensitivity of ET_0 to RH. Zone Ⅱ consistently exhibited the smallest absolute RH sensitivity and relatively limited interannual variability, whereas Zone Ⅰ, Ⅲ, and Ⅳ showed considerably stronger responses to RH.

The sensitivity coefficients of SSD remained positive and relatively stable over time (Figure 5b), indicating a persistent positive response of ET_0

to increased energy availability. Clear differences were observed among subregions: Zone III consistently exhibited the highest SSD sensitivity, whereas Zone IV showed the lowest. In contrast, WIND sensitivity coefficients were positive in all subregions and generally exhibited an increasing tendency over the study period (Figure 5d), particularly in Zone II. This pattern indicates that the relative response of ET_0 to changes in aerodynamic conditions may have strengthened over time. Notably, this increasing sensitivity occurred simultaneously with the long-term decline in WIND identified in Section 3.2, suggesting that reductions in WIND may exert an increasingly important suppressing effect on ET_0, although their actual contribution depends on both sensitivity and the magnitude of the observed WIND trend.

TEM exhibited the weakest sensitivity among the four meteorological factors but showed the greatest regional variability in response direction (Figure 5c). The sensitivity coefficients were predominantly positive in Zones I–III, indicating that increases in temperature generally enhanced ET_0 under these climatic conditions. In contrast, Zone IV was characterized by predominantly negative normalized temperature sensitivity coefficients. This anomalous pattern should be interpreted cautiously. Because the normalized sensitivity coefficient depends on both the derivative of ET_0 with respect to temperature and the magnitude of the temperature itself, the use of temperature expressed in degrees Celsius can produce negative normalized coefficients when mean temperatures approach or fall below 0 °C. Therefore, the negative temperature sensitivity observed in the high-latitude Zone IV does not necessarily imply that physical warming directly reduces ET_0 and may partly reflect the normalization procedure under cold climatic conditions.

The spatial distributions shown in Figure 6 further demonstrate pronounced regional heterogeneity in ET_0 sensitivity. RH exhibited the largest absolute sensitivity coefficients across most of Northeast China, whereas TEM generally showed the smallest values. Based on the regional averages in Table 3, the overall sensitivity ranking was approximately $|s_{RH}| > s_{WIND} > s_{SSD} > |s_{TEM}|$. However, this ordering differed among subregions. Zone II exhibited the highest WIND sensitivity (0.3124) and the lowest absolute RH sensitivity (0.6996), indicating a relatively strong aerodynamic control on ET_0. In contrast, Zone III had a higher SSD sensitivity (0.2875) than WIND sensitivity (0.2136), suggesting that ET_0 in the humid eastern mountainous region was relatively more responsive to variations in energy availability than to aerodynamic forcing. Subregion IV showed the largest absolute RH sensitivity (1.2531), indicating particularly strong dependence of ET_0 on atmospheric moisture conditions in the high-latitude region.

Overall, the sensitivity analysis demonstrates that the climatic controls on ET_0 differ substantially among the K-means-derived subregions. More importantly, sensitivity represents the potential response of ET_0 to changes in individual meteorological factors rather than their actual contribution to the observed ET_0 trend. A meteorological factor may exhibit high sensitivity but only a small long-term change, whereas a moderately sensitive factor may make a substantial contribution if its long-term trend is large (Yu et al., 2002; Wang et al., 2021). Therefore, the contribution analysis in the following section combines the sensitivity coefficients with the observed relative changes in each meteorological factor to identify the dominant drivers of regional ET_0 variations.

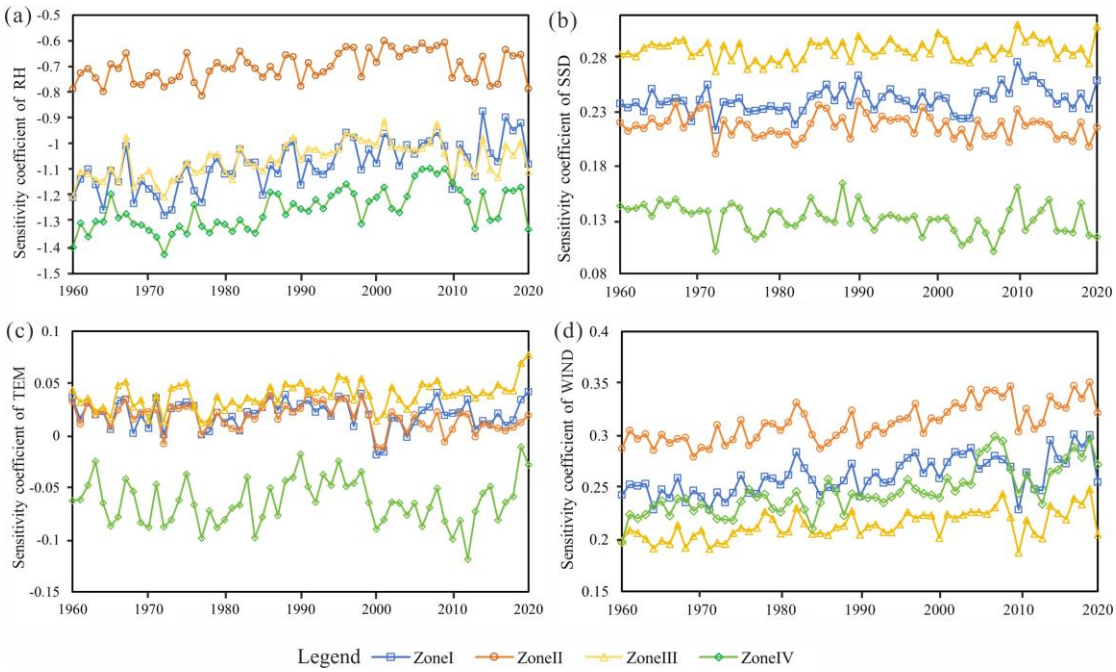


Fig.5 Temporal variations of sensitivity coefficients for meteorological factors across subregions in Northeast China

Table 3. Sensitivity coefficients of meteorological factors by subregion in Northeast China

Meteorological factors	Zone Ⅰ	Zone Ⅱ	Zone Ⅲ	Zone Ⅳ	Overall
RH	-1.078	-0.700	-1.059	-1.253	-1.040
SSD	0.242	0.217	0.288	0.131	0.234
TEM	0.021	0.018	0.038	-0.063	0.011
WIND	0.261	0.312	0.214	0.246	0.249

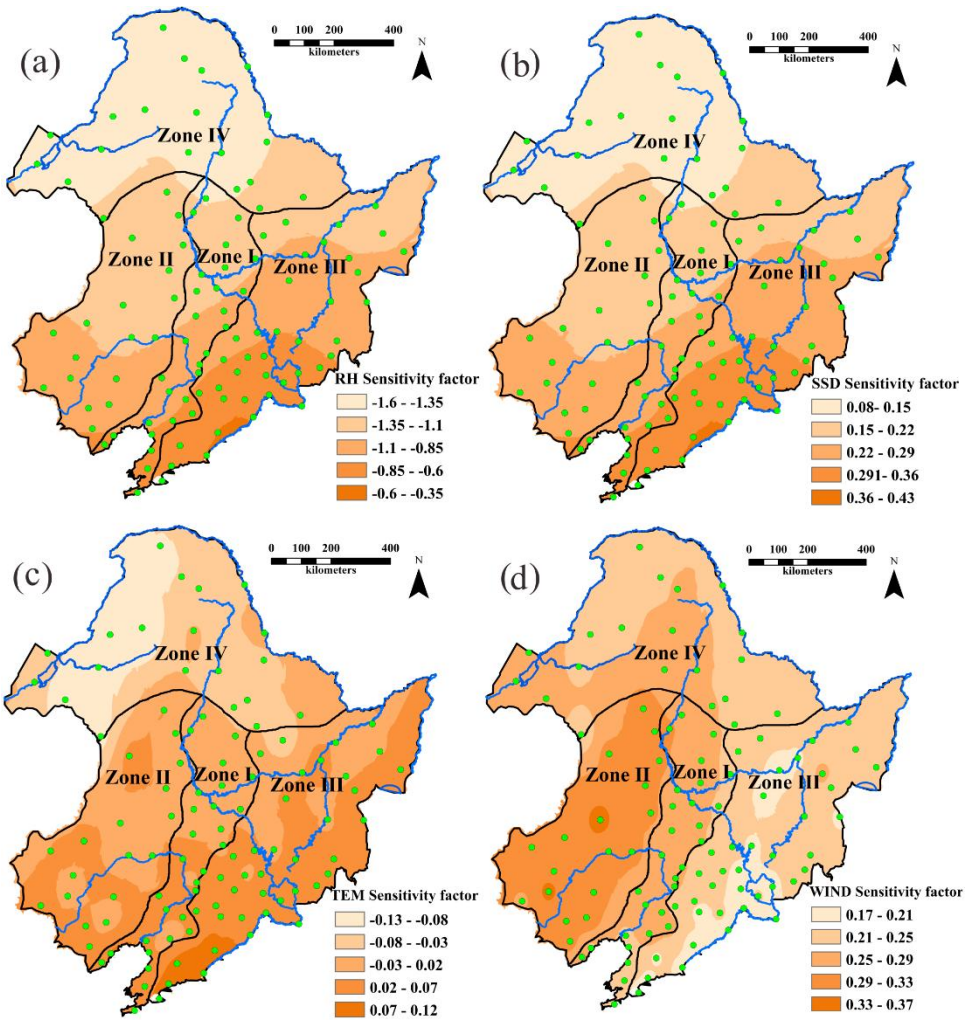


Fig.6 Spatial distribution of sensitivity coefficients for meteorological factors

3.5 Regional Contributions of Meteorological Factors to ET_0 Changes

The contribution analysis combined the sensitivity coefficients with the long-term relative changes in individual meteorological factors to evaluate their roles in regional ET_0 variations (Table 4). In contrast to sensitivity analysis, which reflects the potential response of ET_0 to a unit relative change in a meteorological factor, the contribution rate incorporates both the sensitivity of ET_0 and the magnitude and direction of the observed climatic trend (Zhang et al., 2021). Therefore, a highly sensitive factor does not necessarily make the largest contribution if its long-term change is small, whereas a moderately sensitive factor may exert a substantial influence when it undergoes a pronounced long-term change.

Clear regional differences were observed in the contributions of meteorological factors. In Zone Ⅰ, the long-term decline in WIND produced the largest negative contribution to ET_0 (−11.975%), followed by the negative contribution of declining SSD (−1.904%). In contrast, decreases

in RH produced a positive contribution (2.982%), because ET_0 responds negatively to RH, while increasing TEM also contributed positively (0.550%). The coexistence of positive thermal and humidity effects and stronger negative aerodynamic and radiation effects is consistent with the weak decreasing ET_0 trend observed in this subregion. These results indicate that the decline in ET_0 in the central plain cannot be attributed to cooling but instead reflects the offsetting effects of concurrent changes in atmospheric moisture, wind conditions, and available energy (Liu et al., 2022).

A similar competition among climatic effects occurred in Zone II. Declining RH and increasing TEM favored higher ET_0, whereas reductions in WIND and SSD exerted suppressing effects. The substantial decrease in WIND represents the strongest negative contribution in this subregion. This result is particularly noteworthy because Zone II exhibited the highest WIND sensitivity among the four subregions. Thus, although the mean ET_0 of Zone II was relatively high, the persistent weakening of aerodynamic forcing substantially offset the positive effects associated with warming and decreasing humidity, resulting in an overall weak ET_0 trend.

Zone III showed a different relationship between the calculated contributions and the observed ET_0 trend. The decrease in WIND provided the largest negative contribution (−6.446%), while declining SSD also suppressed ET_0 (−1.490%). Conversely, decreasing RH and increasing TEM contributed positively by 2.386% and 1.324%, respectively. Although the observed ET_0 trend was slightly positive, the sum of the individual first-order contributions was negative. This mismatch indicates that the observed ET_0 variation cannot be fully reconstructed by a simple additive combination of long-term mean sensitivity coefficients and linear climatic trends. Nonlinear interactions among meteorological variables and temporal changes in the sensitivity coefficients may therefore be particularly important in this humid eastern mountainous region.

Zone IV exhibited the strongest observed increase in ET_0, together with pronounced warming and decreasing RH. RH produced a substantial positive contribution because its long-term decline enhanced atmospheric evaporative demand, whereas decreasing WIND and SSD exerted negative effects. The contribution associated with TEM requires cautious interpretation, because the multi-year mean temperature of this high-latitude region is close to or below 0 °C. Consequently, calculating a relative temperature change using temperature expressed in degrees Celsius produces an unstable percentage and may alter the sign and magnitude of the normalized temperature contribution. The TEM contribution in Zone IV should therefore be recalculated or evaluated using an alternative temperature perturbation metric before its physical role is interpreted.

At the regional scale, the opposing contributions of meteorological factors explain why Northeast China as a whole exhibited only a weak ET_0 trend despite significant warming. Declining RH tended to enhance ET_0, whereas reductions in WIND and SSD generally suppressed it. TEM exerted a comparatively small positive contribution over most of the study region. The near cancellation of these competing effects indicates that long-term ET_0 evolution in Northeast China is controlled by the balance among thermal, moisture, radiative, and aerodynamic forcing rather than by temperature change alone (Luo et al., 2021). This mechanism also provides a climatic explanation for the apparent evaporation paradox observed in some subregions, where significant warming did not correspond to an increase in ET_0.

More importantly, discrepancies between the observed ET_0 changes and the sum of individual contribution estimates indicate limitations of a purely additive attribution framework (Nie et al., 2022). Because the Penman–Monteith formulation is nonlinear and the sensitivity coefficients themselves vary with the background climatic state, interactions among climatic variables and temporal changes in sensitivity may generate residual variations that are not captured by contributions calculated from long-term mean coefficients. These unexplained components should therefore be interpreted as evidence of nonlinear and interacting climatic controls rather than being directly attributed to non-meteorological factors.

Table 4. Contribution rates of meteorological factors to ET_0 variations.

Zone	Meteorological factors	WIND	RH	TEM	SSD	ET_0
I	$Trend_{vi}$	-0.025	-0.029	0.030	-0.010	-0.537
	RC_{vi} (%)	-45.935	-2.765	26.460	-7.886	-3.391
	C_{vi} (%)	-11.975	2.982	0.550	-1.904	
II	$Trend_{vi}$	-0.015	-0.036	0.029	-0.007	-0.063
	RC_{vi} (%)	-31.428	-4.171	28.736	-5.357	-0.371
	C_{vi} (%)	-9.818	2.918	0.514	-1.163	
III	$Trend_{vi}$	-0.013	-0.025	0.028	-0.006	0.076
	RC_{vi} (%)	-30.178	-2.252	34.472	-5.182	0.586
	C_{vi} (%)	-6.446	2.386	1.324	-1.490	
IV	$Trend_{vi}$	-0.011	-0.067	0.039	-0.003	0.747
	RC_{vi} (%)	-26.554	-6.162	370.094	-2.548	6.344
	C_{vi} (%)	-6.530	7.722	-23.427	-0.334	
Overall	$Trend_{vi}$	-0.016	-0.036	0.031	-0.006	0.012
	RC_{vi} (%)	-34.735	-3.428	40.458	-5.479	0.081
	C_{vi} (%)	-8.663	3.566	0.441	-1.279	

3.6 Mechanisms Underlying Regional Evaporation-Paradox-Like Responses

The results presented above indicate that Zones I and II exhibited an evaporation paradox-like phenomenon, characterized by significant

warming trends but decreasing or insignificant changes in ET_0. Such a phenomenon suggests that increasing air temperature alone cannot explain long-term variations in atmospheric evaporative demand. Instead, the final response of ET_0 depends on the combined effects of multiple climatic factors and their temporal changes.

Previous studies have demonstrated that the occurrence of the evaporation paradox is closely related to variations in radiation, humidity, and aerodynamic conditions. For example, reduced solar radiation associated with increased cloud cover or aerosol loading has been reported to weaken evaporative demand despite rising temperatures (Wang et al., 2020; Du et al., 2022). Similarly, reductions in wind speed can decrease turbulent exchange and suppress evaporation, thereby offsetting the enhanced evaporative demand caused by warming (Qin et al., 2021). These mechanisms are consistent with the results of this study, where the positive contributions of increasing TEM and decreasing RH in Zones Ⅰ and Ⅱ were insufficient to compensate for the negative contributions associated with declining WIND and SSD.

The occurrence of the evaporation paradox in different regions may also depend on background climatic conditions and the relative importance of individual meteorological controls (Nie et al., 2023; Zhao et al., 2021). In Zone I, the highest WIND among the four subregions and its significant long-term decline resulted in a strong negative contribution to ET_0. Although warming and decreasing RH enhanced atmospheric evaporative demand, the weakening of aerodynamic forcing and radiation availability limited the overall increase in ET_0 (Sabino et al., 2023). In Zone Ⅱ, ET_0 was particularly sensitive to WIND, and the substantial decline in WIND provided the dominant negative contribution. This indicates that aerodynamic constraints played an important role in regulating ET_0 changes in this mountainous continental region.

It should be noted that the contribution analysis based on meteorological factors does not fully capture all possible influences on long-term evapotranspiration-related processes. The Penman–Monteith formulation is nonlinear, and the sensitivity coefficients vary with background climatic conditions. Therefore, interactions among meteorological variables and temporal changes in sensitivity may generate residual variations that cannot be completely explained by individual contribution rates. Previous studies have suggested that vegetation dynamics, atmospheric CO_2 enrichment, and land-use changes may influence actual evapotranspiration through biological and surface processes (Ficklin et al., 2009) . However, their effects on reference evapotranspiration remain indirect and require additional observations or

modeling approaches for verification.

Overall, the evaporation paradox observed in Zones I and II was primarily associated with the competition between warming-enhanced evaporative demand and the suppressing effects of declining aerodynamic and radiative conditions. These results highlight that regional ET_0 responses under climate change are governed not only by temperature trends but also by the combined interactions among humidity, wind speed, and energy availability.

4. Conclusions

(1) Climate-based K-means clustering effectively identified four homogeneous subregions in Northeast China, corresponding well with regional differences in topography and hydrothermal conditions. The results demonstrate that objective climate-based zoning provides a physically meaningful framework for investigating spatial heterogeneity in ET_0 responses compared with traditional geographical divisions.

(2) Northeast China experienced significant warming during 1960–2020, accompanied by decreasing trends in wind speed, relative humidity, and sunshine duration. However, ET_0 responses were spatially heterogeneous: Zones I and II showed weak decreasing trends, Zone III exhibited a slight increase, and Zone IV showed a significant increase. These results indicate that regional warming does not necessarily result in enhanced ET_0 because multiple climatic factors jointly regulate atmospheric evaporative demand.

(3) Sensitivity analysis demonstrated that relative humidity was the most influential factor controlling ET_0 responses, followed by wind speed and sunshine duration, whereas temperature generally exhibited weaker sensitivity. The negative temperature sensitivity observed in the high-latitude Zone IV should be interpreted cautiously, as it may partly result from the normalization method under cold climatic conditions rather than indicating a direct negative physical relationship between warming and ET_0.

(4) Contribution analysis revealed that the dominant drivers of ET_0 variations differed among subregions. Although decreasing humidity and increasing temperature generally promoted ET_0 increases, declining wind speed and sunshine duration provided substantial negative contributions in some regions. The competition among thermal, aerodynamic, moisture, and radiation effects explains the evaporation paradox-like phenomenon observed in Zones I and II. Overall, ET_0 changes in Northeast China are controlled by the combined interactions of multiple climatic factors, emphasizing the need for regionalized assessments of evapotranspiration responses under future climate change.

726

References

Allen RG, Pereira LS, Raes D, Smith M (1998) Crop evapotranspiration-Guidelines for computing crop water requirements-FAO Irrigation and drainage paper 56. Fao, Rome, 300(9):D05109

Aschale TM, Peres DJ, Gullotta A, Sciuto G, Cancelliere A (2023) Trend Analysis and Identification of the Meteorological Factors Influencing Reference Evapotranspiration. Water 15(3):470. https://doi.org/10.3390/w15030470

Chattopadhyay N, Hulme M (1997) Evaporation and potential evapotranspiration in India under conditions of recent and future climate change. Agric For Meteorol 87(1):55–73. https://doi.org/10.1016/S0168-1923(97)00006-3

Dinpashoh Y, Jhajharia D, Fakheri-Fard A, Singh VP, Kahya E (2011) Trends in reference crop evapotranspiration over Iran. J Hydrol 399(3–4):422–433. https://doi.org/10.1016/j.jhydrol.2011.01.021

Dikbas F, Firat M, Koc AC, Gungor M (2013) Defining homogeneous regions for streamflow processes in Turkey using a K-means clustering method. Arab J Sci Eng 38(6):1313–1319. https://doi.org/10.1007/s13369-013-0542-0

Du Y, Zhao J, Huang Q (2022) Quantitative driving analysis of climate on potential evapotranspiration in Loess Plateau incorporating synergistic effects. Ecol Indic 141:109076. https://doi.org/10.1016/j.ecolind.2022.109076

Fang W, Huang S, Huang G, Huang Q, Wang H, Wang L, Zhang Y, Li P, Ma L (2019) Copulas-based risk analysis for inter-seasonal combinations of wet and dry conditions under a changing climate. Int J Climatol 39(4):2005–2021. https://doi.org/10.1002/joc.5929

Ficklin DL, Luo Y, Luedeling E, Zhang M (2009) Climate change sensitivity assessment of a highly agricultural watershed using SWAT. J Hydrol 374(1):16–29. https://doi.org/10.1016/j.jhydrol.2009.05.016

Guo D, Westra S, Maier HR (2017) Sensitivity of potential evapotranspiration to changes in climate variables for different Australian climatic zones. Hydrol Earth Syst Sci 21(4):2107–2126. https://doi.org/10.5194/hess-21-2107-2017

Ghiami-Shomami F, Kawasaki K, Leonardo S, Shinoda S, Fan Y (2019) Sensitivity of potential evapotranspiration to climate factors in forested mountainous watersheds. Hydrol Res Lett 13(3):41–48. https://doi.org/10.3178/hrl.13.41

Ghafouri-Azar M, Lee SI (2023) Meteorological Influences on Reference Evapotranspiration in Different Geographical Regions. Water 15(3):454. https://doi.org/10.3390/w15030454

Hu H, Liu J, Zhang X, Fang M (2023) An effective and adaptable K-means algorithm for big data cluster analysis. Pattern Recognit 139:109404. https://doi.org/10.1016/j.patcog.2023.109404

Ikotun AM, Ezugwu AE, Abualigah L, Abuhaija B, Heming J (2023) K-means clustering algorithms: A comprehensive review, variants analysis, and advances in the era of big data. Inf Sci 622:178–210. https://doi.org/10.1016/j.ins.2022.11.139

Liu Q, Yang Z, Cui B, Sun T (2010) The temporal trends of reference evapotranspiration and its sensitivity to key meteorological variables in the Yellow River Basin, China. Hydrol Process 24(15):2171–2181. https://doi.org/10.1002/hyp.7649

Liu X, Liu C, Liu X, Li C, Cai L, Dong M (2022) Spatial and temporal variation in reference evapotranspiration and its climatic drivers in Northeast China. Water, 14 (23), 3911. https://doi.org/10.3390/w14233911

Li C, Wu P, Li X, Zhou T, Sun S, Wang Y, Luan X, Yu X (2017) Spatial and temporal evolution of climatic factors and its impacts on potential evapotranspiration in

Loess Plateau of Northern Shaanxi, China. Sci Total Environ 589:165–172. https://doi.org/10.1016/j.scitotenv.2017.02.122
Liang L, Li L, Zhang L, Li J, Li B (2008) Sensitivity of Penman-Monteith Reference Crop Evapotranspiration in Tao'er River Basin of Northeastern China. Chin Geogr Sci (4):340–347. https://doi.org/10.1007/s11769-008-0340-x
Luo Y, Gao P, Mu X (2021) Influence of Meteorological Factors on the Potential Evapotranspiration in Yanhe River Basin, China. Water 13(9):1222. https://doi.org/10.3390/w13091222
MacQueen J (1967) Some methods for classification and analysis of multivariate observations. In: Proceedings of the Fifth Berkeley Symposium on Mathematical Statistics and Probability, Volume 1: Statistics. University of California Press, Berkeley, pp 281–298
McCuen RH (1974) A sensitivity and error analysis of procedures used for estimating evaporation. J Am Water Resour Assoc 10(3):486–497. https://doi.org/10.1111/j.1752-1688.1974.tb00590.x
Nie T, Yuan R, Liao S, Zhang Z, Gong Z, Zhao X, Chen P, Li T, Lin Y, Du C, Dai C, Jiang H (2022) Characteristics of potential evapotranspiration changes and its climatic causes in Heilongjiang Province from 1960 to 2019. Agriculture 12(12):2017. https://doi.org/10.3390/agriculture12122017
Nie F, Li Z, Wang R, Li X (2023) An effective and efficient algorithm for K-means clustering with new formulation. IEEE Trans Knowl Data Eng 35(4):3433–3443. https://doi.org/10.1109/TKDE.2022.3155450
Onyutha C (2016) Statistical analyses of potential evapotranspiration changes over the period 1930–2012 in the Nile River riparian countries. Agric For Meteorol 226–227:80–95. https://doi.org/10.1016/j.agrformet.2016.05.015
Ozocak M, Akay AO, Esin Aİ, Yurtseven H, Akgul M (2024) A new framework to spatial and temporal drought analysis for 1990–2020 period with Mann–Kendall and innovative trend analysis methods in Turkey. Nat Hazards 120(2):1463–1517. https://doi.org/10.1007/s11069-023-06258-6
Pour SH, Wahab AKA, Shahid S, Ismail ZB (2020) Changes in reference evapotranspiration and its driving factors in Peninsular Malaysia. Atmos Res 246:105096. https://doi.org/10.1016/j.atmosres.2020.105096
Qin M, Zhang Y, Wan S, Yue Y, Cheng Y, Zhang B (2021) Impact of climate change on “evaporation paradox” in province of Jiangsu in southeastern China. PLoS One 16(2):e0247278. https://doi.org/10.1371/journal.pone.0247278
Rim CS (2004) A sensitivity and error analysis for the Penman evapotranspiration model. KSCE J Civ Eng 8(2):249–254. https://doi.org/10.1007/BF02829125
Sen PK (1968) Estimates of the regression coefficient based on Kendall’s tau. J Am Stat Assoc 63(324):1379–1389. https://doi.org/10.1080/01621459.1968.10480934
Shi XR, She DX, Xia J, Liu J (2022) Changes and attribution of potential evapotranspiration in the Three-North Region from 1960 to 2019. Eng J Wuhan Univ 55(10):973–984. https://doi.org/10.14188/j.1671-8844.2022-10-001
Sun C, Zheng Z, Chen W, Wang Y (2020) Spatial and temporal variations of potential evapotranspiration in the Loess Plateau of China during 1960–2017. Sustainability 12(1):354. https://doi.org/10.3390/su12010354
Sabino M, De Souza AP (2023) Global sensitivity of Penman–Monteith reference evapotranspiration to climatic variables in Mato Grosso, Brazil. Earth 4(3):714–727. https://doi.org/10.3390/earth4030038
Vicente-Serrano SM, Azorin-Molina C, Sanchez-Lorenzo A, Revuelto J, Morán-Tejeda E, López-Moreno JI, Espejo F (2014) Sensitivity of reference evapotranspiration to

changes in meteorological parameters in Spain (1961–2011). Water Resour Res 50(11):8458–8480. https://doi.org/10.1002/2014WR015427

Wang Z, Ye A, Wang L, Liu K, Cheng L (2019) Spatial and temporal characteristics of reference evapotranspiration and its climatic driving factors over China from 1979–2015. Agric Water Manag 213:1096–1108. https://doi.org/10.1016/j.agwat.2018.12.006

Wang F, Shao W, Yu H, Kan G, He X, Zhang D, Ren M, Wang G (2020) Re-evaluation of the power of the Mann–Kendall test for detecting monotonic trends in hydrometeorological time series. Front Earth Sci 8:14. https://doi.org/10.3389/feart.2020.00014

Wang W, Guo B, Zhang Y, Zhang L, Ji M, Xu Y, Zhang X, Zhang Y (2021) The sensitivity of the SPEI to potential evapotranspiration and precipitation at multiple timescales on the Huang-Huai-Hai Plain, China. Theor Appl Climatol 143(1–2):87–99. https://doi.org/10.1007/s00704-020-03394-y

Yu PS, Yang TC, Chou CC (2002) Effects of climate change on evapotranspiration from paddy fields in southern Taiwan. Clim Change 54:165–179. https://doi.org/10.1023/A:1015764831165

Yin Y, Wu S, Chen G, Dai E (2010) Attribution analyses of potential evapotranspiration changes in China since the 1960s. Theor Appl Climatol 101(1–2):19–28. https://doi.org/10.1007/s00704-009-0197-7

Zhao J, Xu Z, Singh VP, Zuo D, Li M (2016) Sensitivity of potential evapotranspiration to climate and vegetation in a water-limited basin at the northern edge of Tibetan Plateau. Water Resour Manag 30(13):4667–4680. https://doi.org/10.1007/s11269-016-1446-z

Zhao J, Xia H, Yue Q, Wang Z (2020) Spatiotemporal variation in reference evapotranspiration and its contributing climatic factors in China under future scenarios. Int J Climatol 40(8):3813–3831. https://doi.org/10.1002/joc.6429

Zeng P, Sun F, Liu Y, Feng H, Zhang R, Che Y (2021) Changes of potential evapotranspiration and its sensitivity across China under future climate scenarios. Atmos Res 261:105763. https://doi.org/10.1016/j.atmosres.2021.105763

Zhang X, Xiao W, Wang Y, Kang M, Wang H, Huang Y (2021) Sensitivity analysis of potential evapotranspiration to key climatic factors in the Shiyang River Basin. J Water Clim Change 12(7):2875–2884. https://doi.org/10.2166/wcc.2020.225

Zhao Z, Zhou M, Zhang LD, Gu S, Li J (2021) Calculating daily reference evapotranspiration in Erhai Irrigated District with the evaporation paradox in consideration. J Irrig Drain 40(2):125–135. https://doi.org/10.13522/j.cnki.ggps.2020306

Declarations

Acknowledgements

The author would like to express sincere gratitude to Yuqing Cao in Jilin University, for her support and encouragement during the writing of this paper.

Funding

This research was funded by the Science Research Project of Hebei Education Department (ZC2025089)

Author contributions

L.M. wrote the main manuscript text, W.H. reviewed and edited the main manuscript text. Y.R. redrew part of the illustrations in the manuscript and polished the manuscript. All authors reviewed the manuscript.

Data availability

Data are available upon reasonable request.

Competing interests

The authors declare no competing interests.

Ethical Approval

Not applicable.

Consent to Participate

Not applicable.

Consent to Publish

Not applicable.